Appl. Phys. B 60, 573–582 (1995)

Applied Physics B Lasers and Optics

Laser-spectroscopic investigations of the lithium resonance lines

L. Windholz

Institut für Experimentalphysik, Technische Universität Graz, Petersgasse 16, A-8010 Graz, Austria
(Fax: +43-316/812 658, E-mail: WINDHOLZ@fexphds01.tu-graz.ac.at)

Received: 2 May 1994/Accepted: 18 July 1994

Abstract. High-resolution laser-atomic-beam spectroscopy allowed us to investigate the lithium D lines in magnetic and electric fields and to determine hyperfine constants, isotope shifts, scalar and tensor polarizabilities and the absolute transition frequencies with high accuracy. The methods used are discussed and the results are summarized.

PACS: 35.10.Fk; 35.10.Di; 32.30.Jc

During the last years we have investigated the lithium resonance lines ($\approx$6708 Å) under the influence of electric and magnetic fields. We were able to study the splitting and intensity behaviour of the line components, to investigate the transition from Zeeman to Paschen-Back effect, and to determine scalar and tensor polarizabilities with high accuracy. Apart from these results, we have determined the properties of the field-free lines: hyperfine constants and fine-structure splitting. Natural lithium consist of two isotopes, ^{6}Li and ^{7}Li, and we obtained accurate values for the isotope shifts. Using a high-precision lambdameter, we determined absolute values for the transition frequencies.

The hyperfine spectrum of the lithium resonance lines consists of three groups of components shown in Fig. 1. We observe, from left to right, the hyperfine components of ^{6}Li D_1, the ^{6}Li D_2 components together with the more intense components of ^{7}Li D_1 and finally, the components of ^{7}Li D_2. The intensities of ^{6}Li and ^{7}Li are caused by the natural abundancy (7.4 and 92.6%). The fine-structure splitting is about 10 GHz and has nearly the same value as the line isotope shift. The hyperfine splitting of $2\,^2P_{3/2}$ is not resolved in the spectrum (^{6}Li $2\,^2P_{3/2}$: $A \approx -1$ MHz, $B \approx -0.1$ MHz; ^{7}Li $2\,^2P_{3/2}$: $A \approx -3$ MHz, $B \approx 0.2$ MHz).

Experimentally, there are mainly two difficulties. On the one hand, the fine-structure splitting and the isotope shift are roughly 10 GHz. To obtain accurate values of such difference frequencies, one has to use a very carefully calibrated marker etalon in order to avoid systematic errors. On the other hand, the hyperfine splitting of the $^2P_{3/2}$ levels is very small, even smaller than the observed line width. Therefore, a straightforward determination from field-free spectra is impossible.

1 Experimental arrangement

1.1 Laser system, atomic-beam apparatus and field assemblies

The laser system used consists of a Coherent 699-21 ring dye laser, slightly modified in some mechanical parts and in the scanning electronics, operated with DCM with a typical output power of 200 mW when pumped with 6 W of the Ar^+-laser line at 488 nm. Part of the laser beam was used for the usual diagnostic: a spectrum analyzer with a Free Spectral Range (FSR) of 2 GHz, a marker etalon (Sect. 1.2), a home-made lambdameter [1] with a resolution of 1 GHz for determing the start wavelength of the scans, and the high-precision lambdameter (Sect. 1.2).

The atomic beam, properly collimated (1:400), was crossed perpendicularly by the exciting-laser beam. To obtain a good signal-to-noise ratio, we had to avoid carefully scattered laser radiation reaching the detector. This was not easy when both the atomic beam and the laser beam had to pass the gap between two electrodes, spaced some tenths of a millimetre, in order to produce high electric fields. So, the atomic beam was chopped within the vacuum system and the photomultiplier signal was amplified using the lock-in technique. When reducing the power of the exciting-laser light to approximately 50 μW, we observed with this arrangement a linewidth of 12–15 MHz, due to the remaining Doppler broadening (compare with the natural linewidth of 5.8 MHz).

For detection in external fields, we have used different field assemblies. The arrangement for investigations in

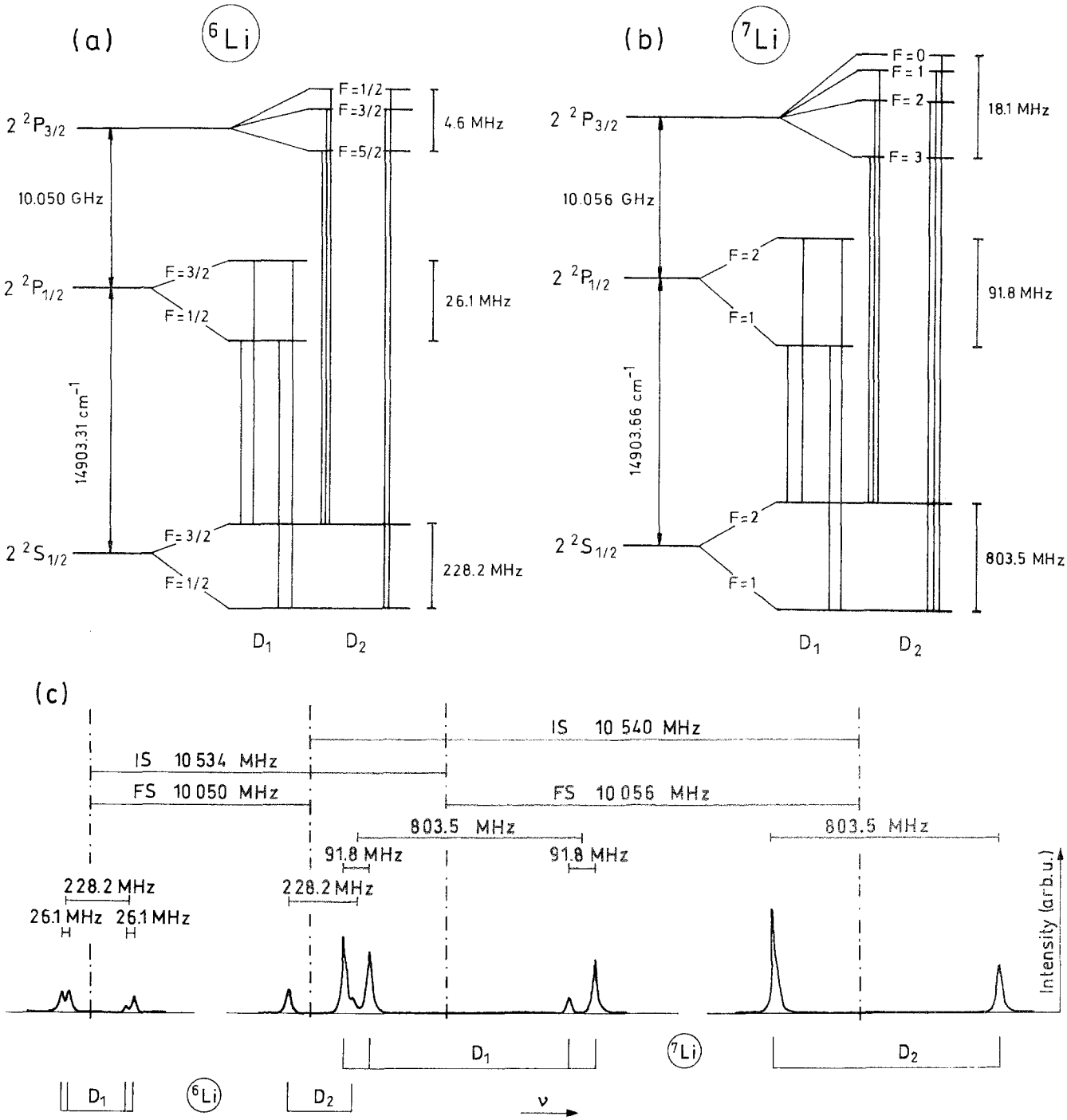

Fig. 1a–c. Hyperfine level scheme of ^{6}Li (**a**), ^{7}Li (**b**) (not to scale) and field-free spectrum (**c**). The hyperfine structures due to the splittings of ^{6}Li $^2P_{3/2}$ and ^{7}Li $^2P_{3/2}$ are not resolved

weak magnetic fields consisted of a pair of Helmholtz coils outside the aluminium vacuum chamber [2]. For high magnetic fields, we set up a large electromagnet with iron pole pieces and an iron yoke [3]. The atomic beam entered the interaction region parallel to the field direction by a bore in one of the cylindrical pole pieces. The magnetic-flux density was measured by means of a Nuclear Magnetic Resonance (NMR) Gaussmeter (accuracy $\pm 10\,\mu$T or ± 0.1 G). For investigations in electric fields, we used two different arrangements. In the high-field arrangement [4], allowing application of electric fields up to 500 kV/cm, the field plates were made of stainless steel, with a diameter of 10 mm and a spacing of ≈ 0.4 mm. The accuracy of the determination of the field strength was limited mainly by the mechanical measurement of the plate spacing to approximately 2%. The second arrangement allowed us to perform investigations in high precisely known fields up to 100 kV/cm. A sketch of the whole assembly used is shown in Fig. 2. We replaced the field electrodes by the plates of a Fabry-Perot Interferometer (FPI) which could be adjusted from outside the vacuum system. To yield electric conductivity, the plates were coated with a silver layer that provided a finesse of the interferometer between 10 and

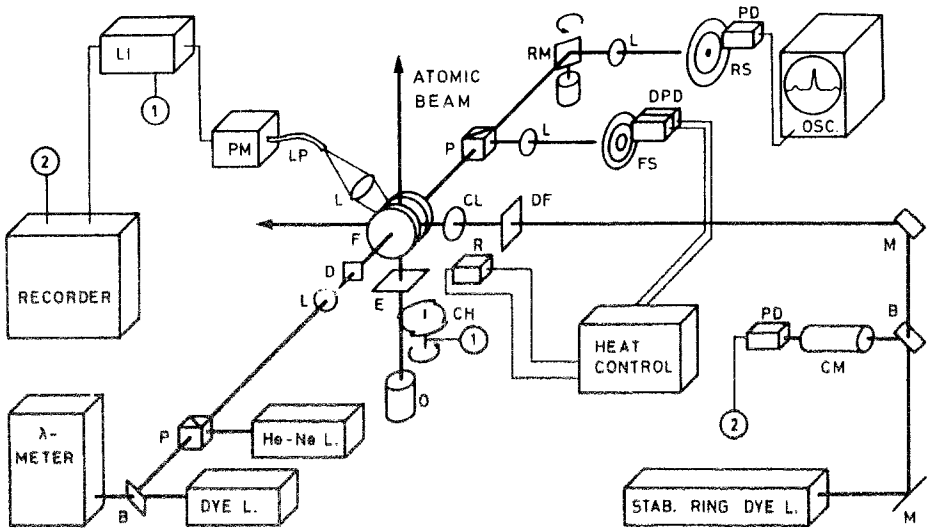

Fig. 2. Experimental arrangement for laser–atomic-beam spectroscopy with the high-precision electric-field assembly. *O*: oven; *CH*: chopper; *E*: entrance aperture of the atomic beam; *F*: field plates forming a FPI (adjustable by micrometer screws from outside the vacuum system, spacing 0.5–0.7 mm); *M*: mirror; *B*: beam splitter; *CM*: confocal marker etalon (oven stabilized); *PD*: photodiode; *DF*: density filters; *CL*: cylindrical lens; *L*: lens; *LP*: light pipe; *PM*: photomultiplier; *LI*: lock-in amplifier; *P*: polarizing beam splitter cube; *D*: diffusing disc; *FS*: fringe system due to the HeNe laser; *DPD*: difference photodiode mounted off-axis for detection of changes of the diameter of the ring system (its signal is used to control the temperature of the ground body of the field assembly); *R*: resistor for heating the ground body; *RS*: fringe system due to the dye laser; *RM*: rotating mirror for moving the dye-laser-produced ring system over the photodiode (the oscilloscope shows then an intensity profile of the ring system allowing reproducable adjustment of the wavelengths of transmission maxima)

20. This coating limited the field-strength range. The spacing of this FPI was approximately 0.5 mm, corresponding to a FSR of about 3.6 Å (for $\lambda \approx 6000$ Å). Precise determination of the spacing d was based on a measurement of the FSR. First, the wavelength of the dye laser was tuned to a certain transition maximum (order k_1, wavelength λ_1) and then to another maximum (order k_2, wavelength λ_2), while counting $\Delta k = k_2 - k_1$. From the wavelengths, we calculated the corresponding frequencies ν_1 and ν_2, $\nu_{FSR} = (\nu_2 - \nu_2)/\Delta k$ and $d = c/2\nu_{FSR}$. The wavelength of each transition maximum was measured with an accuracy of ± 0.01 Å. We choose $\Delta k = 30$ to obtain an accuracy of $\pm 2 \times 10^{-4}$ for a wavelength difference of ≈ 100 Å. This estimation of the accuracy is valid only as long as the etalon does not show any temperature drifts during the time of measurement, changing the frequencies of the transition maxima of the interferometer. In order to avoid such drifts, we illuminated simultaneously the interferometer with the light of a HeNe laser, producing a ring system. The size of the ring system was kept constant by means of a differential photo diode and a feedback circuit regulating the temperature of the field assembly, serving in this way as an active stabilization of the interferometer spacing. The next problem arose when we tried to find the transition maximum of this low-finesse (10–20) FPI with reproducibility of 1/300 of the FSR. As we reported previously [5], this was possible when looking not only to the transmitted intensity but also to the profile of the fringes, even when illuminating the interferometer with laser light showing some intensity noise. Experimentally, we produced the intensity profile of the dye-laser-caused ring system by means of a rotating mirror.

By this high-precision measurement, we obtained an accuracy of 2×10^{-4} for the field strength using this field assembly. Spectra taken at ≈ 100 kV/cm allowed us to calibrate the high-field assembly by comparing the measured Stark shift of the spectral lines. In this way we reached a higher accuracy for high electric fields than by a direct measurement of the spacing. Further information can be found in [5–10].

1.2 Marker etalon and lambdameter

Measurements of frequency separations in laser spectroscopy are usually performed by recording the transmission signal of a confocal FPI with a FSR between 100 and 500 MHz. In order to measure relatively large frequency separations with low systematic error, one has (i) to avoid temperature drifts of the whole interference pattern and (ii) to calibrate the instrument (usually by a measurement of a well-known hyperfine splitting of certain atomic levels, e.g., the sodium ground level). Our interferometer (FSR = 200 MHz) had an invar spacer and was mounted thermally insulated in an evacuated tube. The tube was heated to 38° C with a temperature uncertainty of ± 0.01° C. For measuring fine structures and isotope shifts of ≈ 10 GHz (Li *D* lines), it was insufficient to calibrate with known splittings of ≈ 2 GHz only. Therefore, we calibrated the marker etalon additionally by means of our high-precision lambdameter. We have tuned the dye laser to transition maxima of the marker etalon and have measured the laser frequency with an accuracy of ± 6 MHz. Extending the wavelength difference stepwise and calculating carefully the possible error in order to determine the difference in interference order (Δk), we finally were able to measure over $\Delta k = 62428$ (between 5890 Å and 5750 Å) and determined the FSR to be 197.5974(3) MHz allowing now

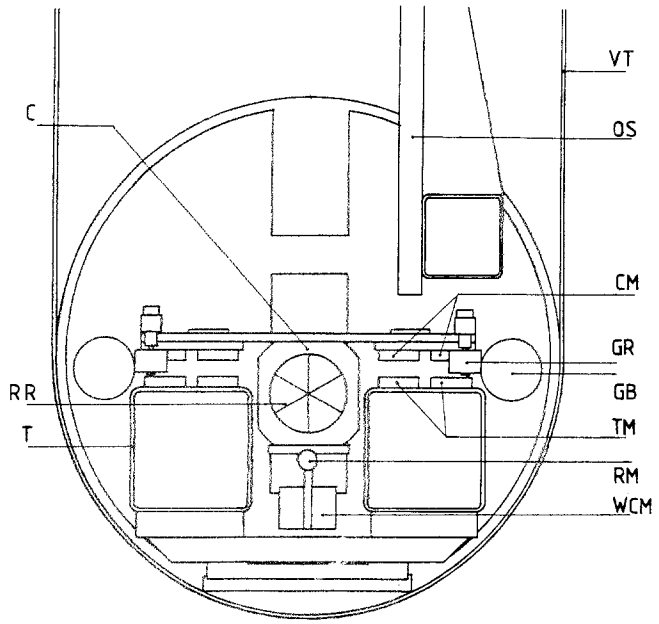

Fig. 3. Cross section view of the high-precision lambdameter. *T:* track; *TM:* track magnets; *GB:* guiding bars; *C:* carriage; *CM:* carriage magnets; *GR:* guiding rollers; *WCM:* weight for positioning the center of mass of the carriage; *RR:* retroreflecting mirrors; *OS:* support for part of the optical components; *VT:* vacuum tank (diameter 250 mm, length 1500 mm)

measurements over 10 GHz with systematic errors smaller than 0.2 MHz [11].

Our high-precision lambdameter is based on a Michelson interferometer. A moving carriage with two retroreflecting mirrors increases the optical length in one arm of the interferometer while decreasing it in the other arm. For a smooth movement of the carriage on its track we choose magnetic levitation using ceramic permanent magnets for vertical support. This kind of support is well suited also when operation in an evacuated environment is demanded, allowing the determination of the vacuum wavelength or the frequency of the laser light without corrections due to the refractive index of air. Nevertheless, it is not possible to obtain a completely stable bearing using only permanent magnets. Therefore, we had to guide the carriage (mass ≈ 2.5 kg) in lateral direction by two steel bars and four Teflon rollers, which exert a force of only 0.3 N to the bars. Friction forces are thus very small and the heavy carriage is running smooth enough to avoid miscounts and to allow a ten-fold electronic frequency multiplication of the count rate of the reference laser, thereby increasing the resolution. The construction can be seen in Fig. 3. The carriage is accelerated at the end of the magnetic track by electromagnetic repulsion and runs then freely with almost constant speed.

The optical arrangement [12] eliminates optical pathlength variations due to angular misalignments and lateral displacements of the carriage (Fig. 4). The change in the optical path length when moving the carriage 0.6 m is 4.8 m. Because of the electronic frequency multiplication used, we obtain a precision of 1/80000000 (at $\lambda = 6000$ Å; $\pm 75 \times 10^{-6}$ Å or ± 6 MHz). The absolute accuracy is not as good since the frequency of the reference laser (polarization-stabilized HeNe-laser, Coherent Tropel 200) is not known exactly. The best value for the transition frequency of the red HeNe-laser line seems to be 473612214.80 (16) MHz [13]. We use the low-frequency component of the laser and have to subtract from this frequency one half of the mode spacing ($1/2 \times 500$ MHz). This leads to a reference frequency of $\nu_{ref} = 473611965$ MHz. Of course, this value is correct only if both polarized components have exact the same intensity. We estimate the systematic error in frequency due to this fact to be ± 30 MHz. Together with the statistical errors in the scans and some minor shifts on the transmission pattern of the marker etalon, we estimate our absolute frequency measurements to be accurate to ± 50 MHz [11, 14].

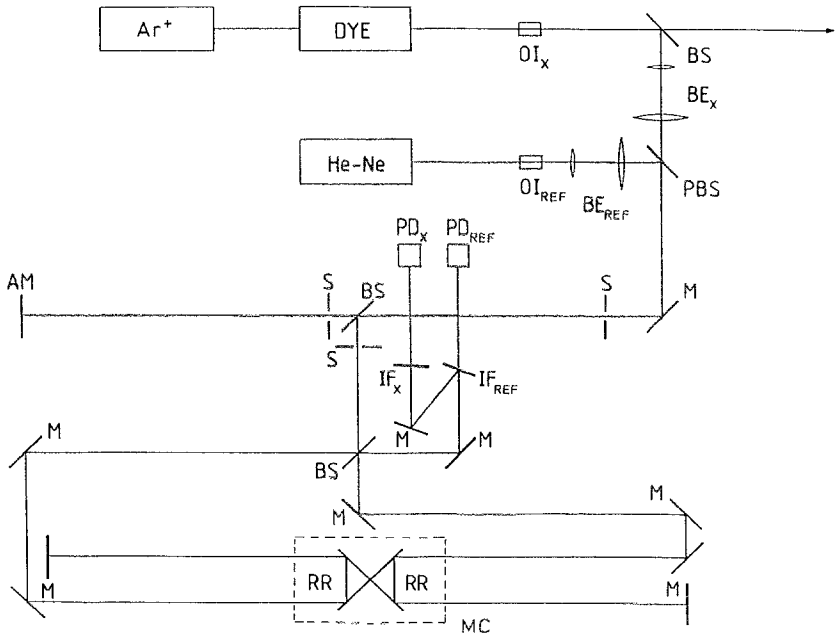

Fig. 4. Optical arrangement of the high-precision lambdameter. *OI:* optical insulator; *BS:* beam splitter; *BE:* beam expander: *PBS:* polarizing beam splitter; *M:* mirror; *S:* beam stop; *AM:* mirror helping when adjusting the interferometer; *RR:* retroreflectors; *MC:* movable carriage; *IF:* interference filter; *PD:* photodiode

2 Data evaluation

The fluorescence spectra were recorded while scanning the laser frequency with typically 500 MHz/min. Simultaneously, we recorded the transmission signal of the marker etalon. Both signals were digitized and stored on a personal computer with a rate of approximatley 5 data points per MHz. In high magnetic fields, the full spectrum consisted of different, widely separated parts. When reaching the first transmission maximum of the marker etalon of such a part, we stopped the laser scan and performed a measurement of the absolute laser frequency by means of our high-precision lambdameter. After this the scan was continued. In such a way, we could easily reconstruct the full spectrum knowing the missing number of frequency marks from the lambdameter reading. Additionally, we determined the transition frequencies from spectra without external field.

The spectra were fitted with Voigt profiles by means of a least-squares procedure [15]. Using the obtained centre frequencies of the spectral components, we were able to determine the physical parameters of the lines. In order to extract parameters from sets of recordings at different magnetic or electric field strength, we fitted the theoretical field pattern to the experimentally observed spectra, handling the desired constants as free parameters in the fitting procedure.

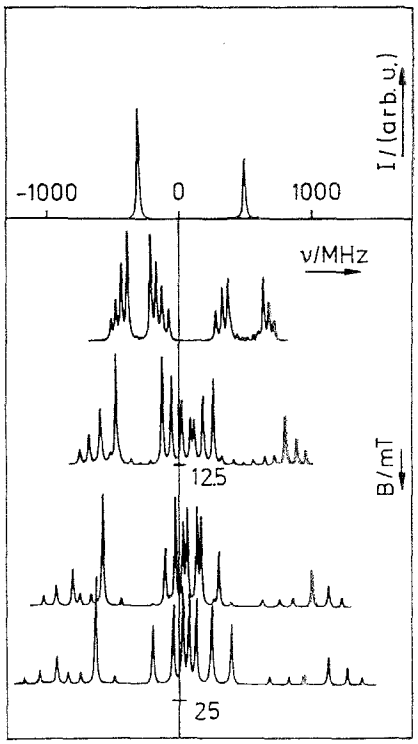

Fig. 5. Zeeman effect of the ^{7}Li D_2 line. Exciting-laser light σ-polarized

3 Results

3.1 Spectra without fields. Hyperfine constants of ^{6}Li $^2S_{1/2}$, $^2P_{1/2}$; ^{7}Li $^2S_{1/2}$, $^2P_{1/2}$

A typical field-free spectrum (field-free means that we have not applied external fields, so only the earth-magnetic field is present) together with the transition scheme is shown in Fig. 1. From such spectra, we determined the hyperfine constants A for the ground level $2\,^2S_{1/2}$ and for the upper level $2\,^2P_{1/2}$ for both isotopes directly from the D_1 lines. Additionally, the splitting of the ground levels was determined from the more intense D_2 lines taking into account slight changes in the center of gravity due to unresolved hyperfine components belonging to $2\,^2P_{3/2}$ (its A and B constants were taken from [16]). The results are listed in Table 1.

3.2 Spectra in magnetic fields. Hyperfine constants of ^{7}Li $^2P_{3/2}$

Computer programs which are based on the diagonalization of the interaction Hamiltonian were developed to analyze complex hyperfine spectra in magnetic, electric and combined fields. These programs allow the calculation of the splittings of ground and excited levels and of the transition probabilities between the different hyperfine components. In this way, a complete simulation of the pattern in external fields is possible. A detailed description can be found in [17], and applications on the complicated cases of simultaneously acting magnetic and electric fields, oriented either parallel or perpendicular to each other, are given in [18, 19].

Spectra in magnetic fields up to 30 mT were recorded in order to study the magnetic splitting of the hyperfine components [11]. Figure 5 shows, as an example, the Zeeman pattern for the ^{7}Li D_2 line, excited by σ-polarized laser light.

For the $2\,^2P_{3/2}$ level, fields larger than 1 mT are "strong", and the components are arranged due to the Paschen-Back effect. For the ground level $2\,^2S_{1/2}$, fields smaller than 10 mT are "weak", and one obtains the Zeeman effect of the hyperfine components. Below 10 mT, we thus obtained a pattern known from literature [20] as "partial Paschen-Back effect". At increasing field strengths, also the components belonging to $2\,^2S_{1/2}$ start to influence each other, and the component groups were more and more overlapping.

From spectra in magnetic fields, we also determined the hyperfine parameters of ^{7}Li $^2P_{3/2}$. The first step was to fit the theoretically obtained field pattern of the D_1 line to the experimental ones, handling the magnetic-flux density B as a free parameter. In this way, we obtained connection factor between B and the current of our Helmholtz coils. Now, we were able to determine the magnetic-flux density for the spectra of the D_2 line. Using a Cern program named 'minuit' [21], we fitted the computed Zeeman pattern to the spectra of the D_2 line, handling in this case the hyperfine constants A and B of $2\,^2P_{3/2}$ as free parameters. With this procedure, we determined A and B with proper errors, as can be seen in Table 1, without directly resolving the small hyperfine splittings in zero fields [11].

Table 1. Values for the hyperfine constants of ^{6}Li and ^{7}Li (ABMR: Atomic-Beam Magnetic Resonance; ODR: Optical Double Resonance; LAB: Laser–Atomic-Beam spectroscopy; QB: Quantum Beats; LC: Level-Crossing spectroscopy; LIF: Laser-Induced Fluorescence; AIC: Ab-Initio Calculations; REV: REView article, average of different measurements, * $A(2\,^2P_{1/2}) = -a_c - 10a_d + 2a_0$; ** $A(2\,^2P_{3/2}) = a_c + a_d + a_0$)

Isotope	Constant (level)	Value [MHz]	Method	Reference
^{6}Li	$A(2\,^2S_{1/2})$	152.1368407(20)	ABMR	[23]
		153.3(11)	LAB	[11]
^{6}Li	$A(2\,^2P_{1/2})$	17.375(18)	ODR	[25]
		17.8(3)	LC	[26]
		16.81(70)	LAB	[11]
^{6}Li	$A(2\,^2P_{3/2})$	−1.155(8)	ODR	[25]
^{6}Li	$B(2\,^2P_{3/2})$	−0.10(14)	ODR	[25]
^{7}Li	$A(2\,^2S_{1/2})$	401.7520433(5)	ABMR	[23]
		401.81(25)	LAB	[11]
^{7}Li	$A(2\,^2P_{1/2})$	46.17(35)	ODR	[27]
		45.914(25)	ODR	[28]
		46.05(30)	LAB	[11]
		46.175*	LAB	[3]
^{7}Li	$A(2\,^2P_{3/2})$	−3.055(14)	ODR	[28]
		−3.24(13)	LC	[29]
		−2.95(4)	LC	[26]
		−3.08(4)	LIF	[30]
		−3.08(8)	QB	[31]
		−3.18(10)	LAB	[11]
		−2.96**	LAB	[3]
^{7}Li	$a_c(2\,^2P_{1/2,\,3/2})$	−9.788(45)	ODR	[28]
		−9.806(117)	LC	[29]
		−9.888(100)	AIC	[34]
		−9.93(37)	LAB	[3]
^{7}Li	$a_d(2\,^2P_{1/2,\,3/2})$	−1.886(25)	ODR	[28]
		−1.909(34)	LC	[29]
		−1.869(20)	AIC	[34]
		−1.72(20)	LAB	[3]
^{7}Li	$a_0(2\,^2P_{1/2,\,3/2})$	8.628(35)	ODR	[28]
		8.638(39)	LC	[29]
		8.728(87)	AIC	[34]
		8.69(31)	LAB	[3]
^{7}Li	$B(2\,^2P_{3/2}) = b$	−0.235(35)	ODR	[28]
		−0.16(10)	LIF	[30]
		−0.20(27)	QB	[31]
		−0.18(12)	REV	[16]
		−0.14(10)	REV	[16]
		−0.8(7)	LAB	[11]
		−0.1(5)	LAB	[3]

3.3 Spectra in strong magnetic fields. Crossing field strengths

At high magnetic-field strengths (for ^{7}Li, $B > 100$ mT), the fine structure levels $2\,^2P_{1/2}$ and $2\,^2P_{3/2}$ start to influence each other. This behaviour results in two level-crossing regions, where the components of $^2P_{3/2}$, $M_J = -3/2$ cross with $^2P_{1/2}$, $M_J = 1/2$ (at about 320 mT) and $M_J = -1/2$ (at about 480 mT) (Fig. 6a). Figure 6b shows the crossing region at 320 mT in more detail. With high-resolution laser spectroscopy, it was possible to study the crossing of the hyperfine components belonging to the values of M_J mentioned above. In the spectra, the level components of Fig. 6b show allowed transitions to different Zeeman components of the ground state $2\,^2S_{1/2}$, and we obtain 4 pairs of line components crossing each other, as shown in Fig. 7a. Exactly at the crossing points, we observed changes in the spatial distribution of the fluorescence light due to level-crossing effects. From the natural line width (≈ 5.8 MHz) and the slope of the crossing components such effects should appear over a range of field strength of ≈ 0.7 mT. Because the laser-line width was much smaller than the natural line width, the field-strength region where we observed such effects was only 0.15 mT, and we could find the crossing points, listed in Table 2, with an accuracy of 0.01 mT [3]. In the second crossing region, we observed mainly level anticrossings. In Fig. 7b, the change in intensity at the anticrossing points can be seen very impressively. In the same way as described above, we used the spectral positions of the line components in strong fields to determine the hyperfine constants. The results are included in

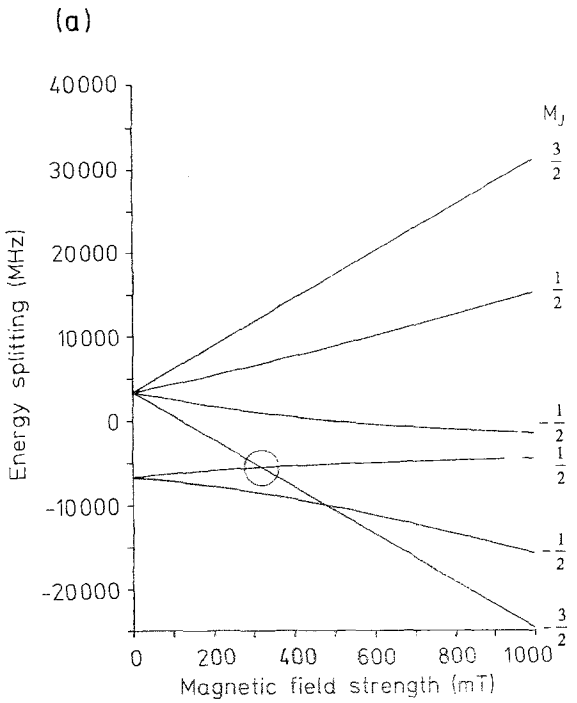

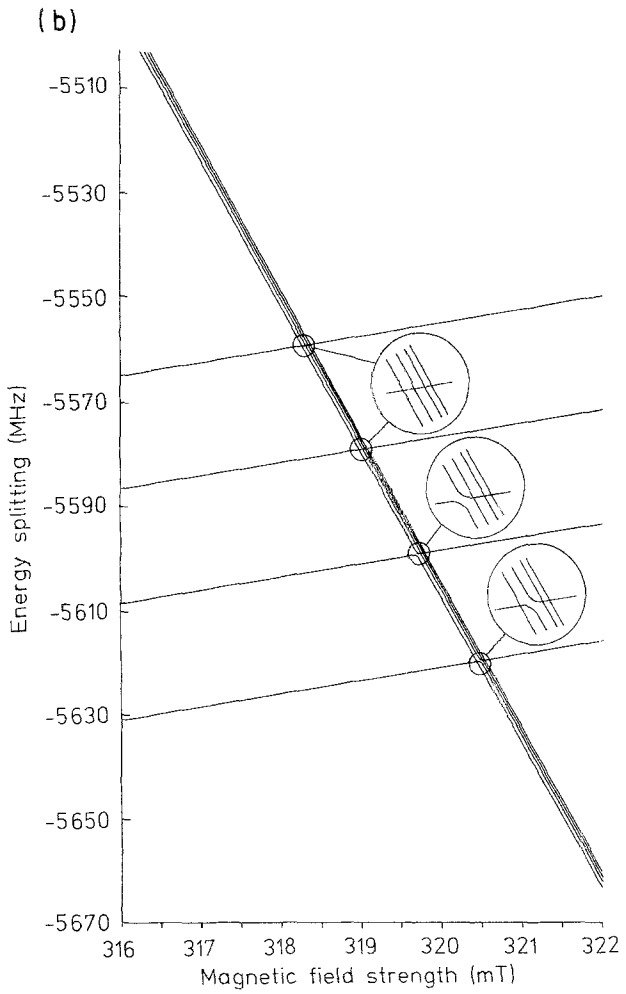

Fig. 6a, b. Zeeman splitting of the Li fine-structure levels $2\,^2P_{1/2}$ and $2\,^2P_{3/2}$ (**a**). The hyperfine levels in the first *(circled)* crossing region around 320 mT show some crossings and anticrossings (**b**)

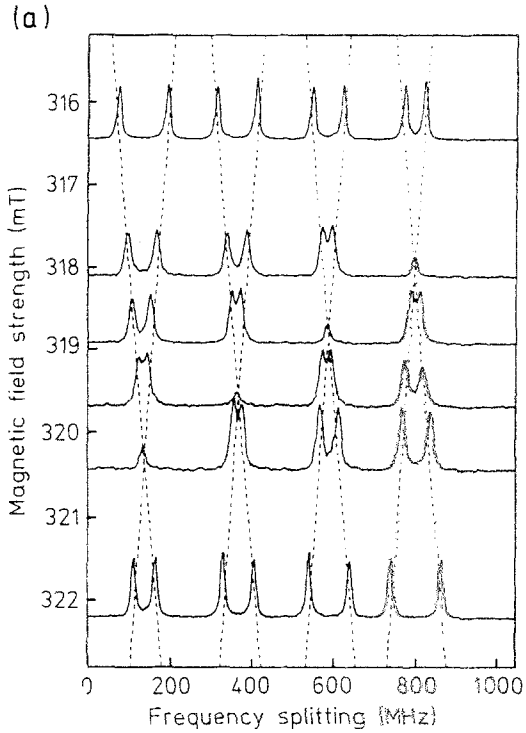

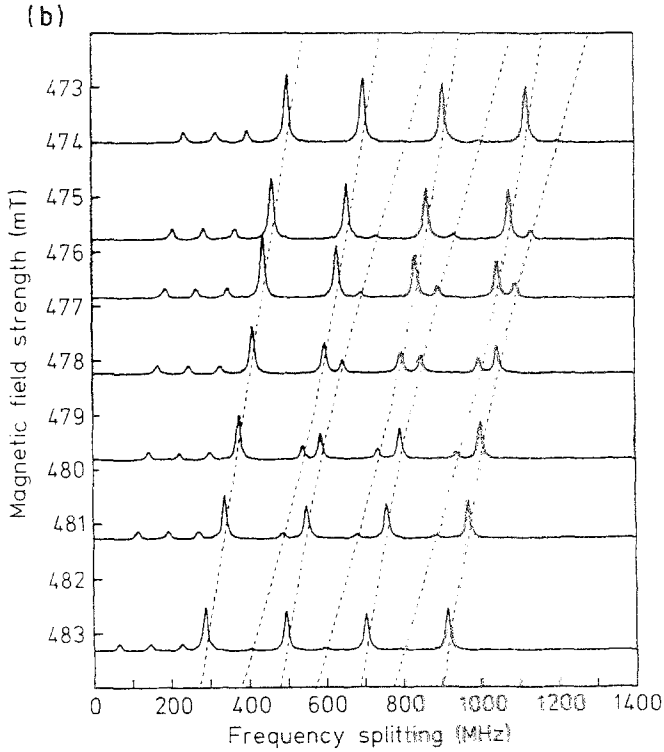

Fig. 7a, b. Spectra of ^{7}Li $2P$–$2S$ components at the crossing regions. Exciting-laser light σ-polarized; direction of observation perpendicular to the atomic beam and to the direction of the magnetic field. Dotted lines show the calculated frequency splittings. **a** In the crossing region around 320 mT. When the field strength is exactly at the crossing point, the intensity of the overlapping components is very small indicating level-crossing effects. **b** In the anticrossing region around 480 mT. The change in intensity between the anticrossing components can be seen clearly

Table 2. Positions of the level-crossing points of ^{7}Li

Level-crossing point no.	B [mT]
1	318.08(1)
2	318.80(1)
3	319.63(1)
4	320.40(1)

Table 3. Fine-structure splitting $^2P_{1/2}-{}^2P_{3/2}$

Isotope	FS-splitting [MHz]	FS-constant ζ [MHz]	Method	Authors
^{6}Li	10050.2(15)	6700.133(10)	LAB	[11]
^{7}Li	10053.184(58)	6702.093(44)	ODR	[28]
	10053.24(22)	6702.16(15)	LC	[35]
	10056.6(15)	6704.4(10)	LAB	[11]
	10053.2(15)	6702.1(9)	LAB	[3]

Table 1. For a better comparison with theoretical calculations, we have used a form of the hyperfine-interaction Hamiltonian which contains four hyperfine constants for the contact, the orbital, the spin-dipolar and the quadrupole term (a_c, a_0, a_d, b).

3.4 Fine-structure splitting and transition isotope shift

Using the hyperfine constants listed in Table 1, we were able to calculate the centers of gravity for the D_1 and D_2 lines of both isotopes. Apart from statistical errors ($\approx \pm 1$ MHz for the center frequencies within one spectrum), we have only negligible systematic errors due to the careful calibration of the marker etalon (cf. Sect. 1). Thus, we observed the fine-structure splitting and the line isotope shift with high accuracy [11]. The results are listed in Tables 3 and 4.

3.5 Spectra in electric fields. Polarizabilities

As pointed out in Sect. 1.1, tremendous experimental effort is necessary to obtain accurate values for the electric-field strength. Of course, for a determination of the polarizabilities, the measurement of the shifts of the spectral lines should have the same relative accuracy. For this reason, the field strength must be high enough to shift the lines some hundreds of MHz. In the case of the lithium resonance lines this is relatively difficult, because their shifts are very small (compare Fig. 8; the line shifts are approximately five times smaller than for the sodium D lines). Additionally, one has to take into account that in high fields the hyperfine pattern of $2\,^2P_{3/2}$ changes compared to the field-free case (Fig. 9). To take into account these changes, we fitted the theoretical Stark spectra to the experimental ones, handling the scalar and tensor polarizabilities as free parameters. Nevertheless, the small shifts and, therefore, the necessary use of the high-field assembly and its calibration caused errors of the polarizabilities of the order of 0.5%. The results are given in Table 5 [4]. It should be mentioned that with laser-spectroscopy methods one is able to determine with high accuracy the difference of the scalar polarizabilities of the ground and excited state ($\alpha_{0,^2P_J}-\alpha_{0,^2S_{1/2}}$), but not the polarizabilities themself, which would be desirable for comparison with theoretical results. In contrary, the

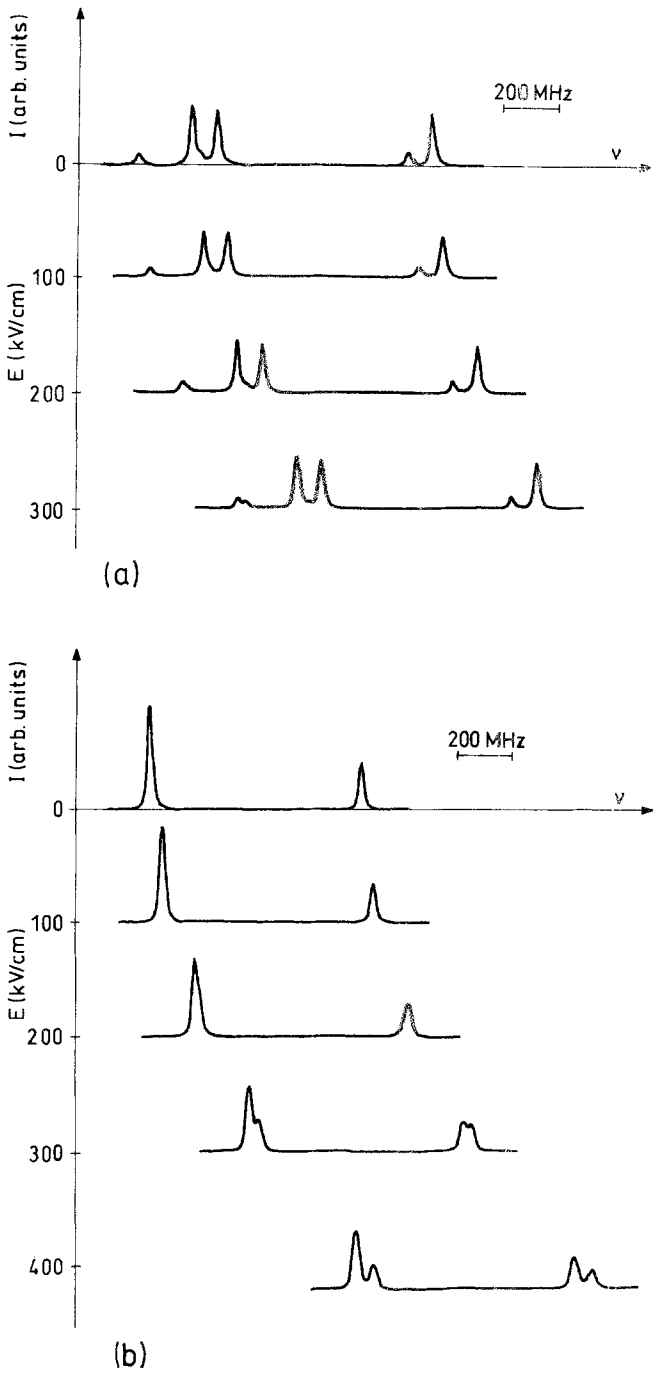

Fig. 8a, b. Spectra in high electric fields. **a** ^{6}Li D_2 and ^{7}Li D_1 line (central part of the spectrum shown in Fig. 1c, and **b** ^{7}Li D_2 line. The D_1 line shows a common shift of its four components. The hyperfine structure of the $^2P_{3/2}$ level of the D_2 line is not resolved and we observe a splitting due to the tensor polarizability α_2

Table 4. Transition isotope shift $2S$–$2P$ (between the centers of gravity of the fine-structure levels)

Isotope pair	Line	IS [MHz]	Method	Reference
^{7}Li–^{6}Li	D_2	10534.8(20)	LAB	[32]
	D_2	10536.45	Theory	[33]
	D_2	10539.9(12)	LAB	[11]
^{7}Li–^{6}Li	D_1?	10532(5)	ODR	[28]
	D_1?	10520(20)	LSP	[36]
	D_1?	10532(5)	?	[37]
	D_1	10536.45	Theory	[33]
	D_1	10534.3(3)	LAB	[11]

Table 5. Scalar and tensor polarizability data (* theoretical data)

Isotope	Line	$(\alpha_{0,^2P_J}-\alpha_{0,^2S_{1/2}})$	α_2	Reference
^{6}Li	D_1	−9.24(15)		[4]
		−9.244(5)		[38]
^{6}Li	D_2	−9.17(17)	0.406(11)	[4]
^{7}Li	D_1	−9.23(8)		[4]
		−9.242(5)		[38]
		−9.272*		[39]
^{7}Li	D_2	−9.28(9)	0.409(11)	[4]

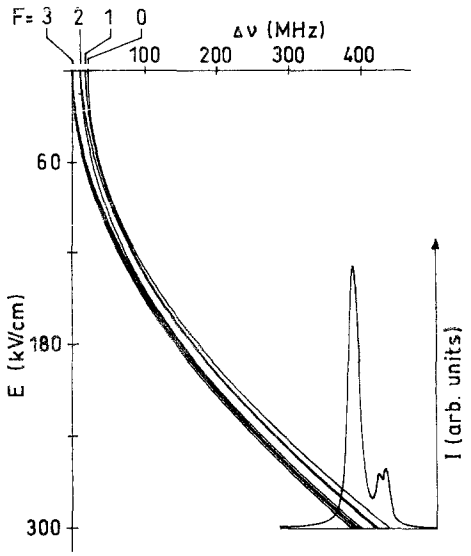

Fig. 9. Calculated Stark splitting of the transition pattern ^{7}Li $2\,^2P_{3/2}$, $(F=3, 2, 1, 0)$–$2\,^2S_{1/2}$, $(F'=2)$ in electric fields up to 300 kV/cm. For 300 kV/cm, the theoretical line profile (exciting-laser light σ-polarized) is shown

tensor polarizabilities α_2, responsible for the splitting of the components of $^2P_{3/2}$, can be determined directly.

3.6 Transition frequencies and wavelengths

In order to determine the absolute transition frequencies of the D lines, we stopped the laser scan when reaching the first maximum of the marker etalon and measured the laser frequency by means of the lambdameter with a precision of ±6 MHz. As mentioned before, the frequency of our reference laser is assumed to be $\nu_{ref}=473\,611\,965(30)$ MHz.

For the ^{7}Li D_2 line, the frequencies of the two component groups $^2P_{3/2}$, $(F=3, 2, 1)$–$^2S_{1/2}$ $(F'=2)$ and $^2P_{3/2}$, $(F=2, 1, 0)$–$^2S_{1/2}$, $(F'=1)$ were determined to be $\nu_1=446\,809\,655$ MHz and $\nu_2=446\,810\,470$ MHz. In order to obtain these values, we had to take into account that the measurements were performed air. So, the output frequencies of our lambdameter had to be corrected by the ratio of the indices of refraction for $\lambda=632.8$ nm and $\lambda=670.8$ nm, $1.000\,276\,516/1.000\,276\,077=1.000\,000\,439$, calculated from the formula given by Peck and Reeder [22] for spectroscopic conditions. The conditions in the laboratory (Graz has an altitude of 370 m, and we had 20° C) do not change this ratio, but we add for this 10 MHz to the errors. The frequency difference $\nu_2-\nu_1$ is 815 MHz. This gives a hyperfine splitting of the ground level of 807 MHz, taking into account a shift of ≈8 MHz in the center of the intensity of the two groups due to the unresolved hyperfine structure of $^2P_{3/2}$, which is in fair agreement with the value determined by atomic-beam magnetic-resonance methods $(2\times 401.7502433(5)\approx 803.5$ MHz) [23].

Using these frequencies, the values for the hyperfine constants and our values for the fine-structure splitting and the isotope shifts [11], we determined the transition frequencies of the centers of gravity for the D lines and the vacuum wavenumbers for both lithium isotopes. From these frequencies, using $n_{air}=1.000\,276\,077$ for the index of refraction of air (at 15° C and 760 mTorr), we also obtained the transition wavelengths. The results are given in Table 6 together with a comparision with results of other authors.

Table 6. Transition frequencies between the fine-structure levels, wave numbers and wavelengths of the *D* lines. The error of the differences between the frequencies given is much smaller: ±1.5 MHz (* vacuum, ** air 15° C, 760 mTorr)

Isotope	Line	Frequency [MHz]	Wavenumber [cm^{-1}]	Wavelength (air) [Å]	Reference
^{6}Li	D_1	446789371(60)	14903.289(2)	6708.076(1)	This work
^{6}Li	D_2	446799421(60)	14903.624(2)	6707.925(1)	This work
^{7}Li	D_1	446799903(60)	14903.640(2)	6707.918(1)	This work
				6707.91(?)	[40]
				6707.912(1)	[41]
			14903.654(2)		[42]
			14903.648(1)		[43]
^{7}Li	D_2	446809659(60)			This work
^{7}Li	D_2	446810466(60)			This work
^{7}Li	D_2	446809961(60)	14903.976(2)	6707.767(1)	This work
				6707.76(?)	[40]
				6707.761(1)	[41]
			14903.990(2)		[42]
			14903.983(1)		[43]
^{7}Li	$D_1 + D_2$			6707.844(5)	[44]

4 Conclusion

Applying external fields and using high-precision calibration methods for the spectroscopic equipment, we investigated nearly all properties of the lithium resonance lines with the help of laser-atomic-beam spectroscopy.

Acknowledgements. I would like to thank all members of the atomic and molecular spectroscopy group at our institute, especially, C. Neureiter, M. Musso, G. Zerza and C. Umfer, for their cooperation and engagement. Without their help it would not have been possible to present all these results. I also acknowledge the continous interest and support of the head of the institute, Prof. Dr. H. Jäger. He helped us with a lot of fruitful and exciting discussions. Parts of the investigations were supported by the Austrian Science Foundation under project numbers P 5806 and P 8273.

References

1. G. Pfeifer, C. Neureiter, L. Windholz: Exp. Techn. Phys. **39**, 161 (1991)
2. L. Windholz: Z. Phys. A **322**, 203 (1985)
3. C. Umfer, L. Windholz, M. Musso: Z. Phys. D **25**, 23 (1992)
4. L. Windholz, H. Jäger, M. Musso, G. Zerza: Phys. Rev. A **46**, 5812 (1992)
5. H. Jäger, M. Musso, C. Neureiter, L. Windholz: Opt. Eng. **29**, 42 (1990)
6. L. Windholz, C. Neureiter: J. Phys. E **17**, 186 (1984)
7. L. Windholz, C. Neureiter: Phys. Lett. **109** A, 155 (1985)
8. L. Windholz, C. Neureiter: In *Laser Spectroscopy VII,* ed. by T.W. Hänsch, Y.R. Shen, Springer Ser. Opt. Sci. Vol. 49 (Springer, Berlin, Heidelberg 1985)
9. C. Neureiter, R.H. Rinkleff, L. Windholz: J. Phys. B **19**, 2227 (1986)
10. L. Windholz, M. Musso: Phys. Rev. A **39**, 2472 (1989)
11. L. Windholz, H. Jäger, M. Musso, G. Zerza: Z. Phys. D **16**, 41 (1990)
12. H.R. Xia, S.V. Benson, T.W. Hänsch: Laser Focus, 54–58 (March 1981)
13. D.J.E. Knight: Metrologia **22**, 251 (1986)
14. M. Musso: Ein Präzisionslambdameter mit magnetisch gelagertem Meßwagen. Diploma Thesis, Technische Universität Graz (1985)
15. W. Schwarz: Entwicklung eines Meßdatenerfassungs- und -Auswertesystems zur laserspektroskopischen Untersuchung der Hyperfeinstruktur der Natrium-D_1-Linie bei hohen Teilchendichten. Diploma Thesis, Technische Universität Graz (1988)
16. E. Arimondo, M. Inguscio, P. Violino: Rev. Mod. Phys. **49**, 31 (1977)
17. M. Musso: Z. Phys. D **24**, 203 (1992)
18. L. Windholz, M. Musso: Z. Phys. D **27**, 229 (1993)
19. L. Windholz, M. Musso: Z. Phys. D (1993) (in press)
20. H. Kopfermann (1956) *Kernmomente,* 2nd edn. (Akademische Verlagsges., Frankfurt 1956)
21. F. James, M. Roos: *Function Minimization and Error Analysis (MINUIT),* CERN Comp. Centre Progr. Library, D506 (CERN, Geneva 1978)
22. E.R. Peck and K. Reeder: J. Opt. Soc. Am. **62**, 958 (1972)
23. A. Beckmann, K.D. Böklen, D. Elke: Z. Phys. **270**, 173 (1974)
24. L. Windholz, C. Umfer: Z. Phys. D **29**, 121 (1994)
25. H. Orth, R. Veit, H. Ackermann, E.W. Otten: Abstracts of Contributed Papers, ed. by J. Kowalski, H.G. Weber, 4th ICAP, Heidelberg (1981)
26. W. Nagourney, W. Happer, A. Lurio: Phys. Rev. A **17**, 1394 (1978)
27. G.J. Ritter: Cdn. J. Phys. **40**, 770 (1965)
28. H. Orth, H. Ackermann, W. Otten: Z. Phys. A **273**, 221 (1975)
29. J.D. Lyons, T.P. Das: Phys. Rev. A **2**, 2250 (1970)
30. F. Shimizu, K. Shimizu, Y. Gomi, H. Takuma: Phys. Rev. A **35**, 3149 (1987)
31. J. Carlsson, L. Sturesson: Z. Phys. D **14**, 281 (1989)
32. M. Fuchs, H.-G. Ruhbahn: Z. Phys. D **1**, 253 (1986)
33. K.T. Chung: Private communication (1994)
34. R.K. Nesbet: Phys. Rev. A **2**, 661 (1970)
35. K.C. Brog, T.G. Eck, H. Wieder: Phys. Rev. **153**, 91 (1967)
36. C. Vadla, A. Obrebski, K. Niemax: Opt. Commun. **63**, 288 (1987)
37. R. Marinella: Appl. Phys. Lett. **35**, 580 (1979)
38. L.R. Hunter, Jr., D. Krause, D.L. Berkeland, M.G. Boshier: Phys. Rev. A **44**, 6140 (1991)
39. J. Pipin, D.M. Bishop: Phys. Rev. A **47**, R4571 (1993)
40. A.N. Zaidel, V.K. Prokofev, S.M. Raiskii, V.A. Slavnyi, E.Ya. Shreider: *Tables of Spectral Lines* (IFI/Plenum, New York 1970)
41. K.W. Meissner, L.G. Mundie, P.H. Stelson: Phys. Rev. **74**, 932 conversion to wave numbers corrected in [42] (1948)
42. I. Johansson: Ark. Fys. **15**, 169 (1959)
43. L.J. Radziemski, C. Sansonetti: Private communication (1994)
44. *Wavelength Tables,* 4th edn. (M.I.T., Cambridge, MA 1985)